

Quantum electric-dipole liquid on a triangular lattice

Shi-Peng Shen¹, Jia-Chuan Wu², Jun-Da Song², Xue-Feng Sun^{2,3,4}, Yi-Feng Yang¹,
Yi-Sheng Chai¹, Da-Shan Shang¹, Shou-Guo Wang¹, James F. Scott⁵ & Young Sun¹

¹Beijing National Laboratory for Condensed Matter Physics, Institute of Physics, Chinese Academy of Sciences, Beijing 100190, China

²Hefei National Laboratory for Physical Sciences at the Microscale, University of Science and Technology of China, Hefei 230026, China

³Key Laboratory of Strongly-Coupled Quantum Matter Physics, Chinese Academy of Sciences, Hefei, Anhui 230026, China

⁴Collaborative Innovation Center of Advanced Microstructures, Nanjing, Jiangsu 210093, China

⁵Cavendish Laboratory, University of Cambridge, J. J. Thomson Avenue, Cambridge, CB3 0HE, UK

Geometric frustrations and quantum mechanical fluctuations may prohibit the formation of long-range ordering even at the lowest temperature, and therefore liquid-like ground states could be expected. A good example is the quantum spin liquid in frustrated magnets that represents an exotic phase of matter and is attracting enormous interests¹⁻³. Geometric frustrations and quantum fluctuations can happen beyond magnetic systems. Here we propose that quantum electric-dipole liquids, analogs to quantum spin liquids, could emerge in frustrated dielectrics where antiferroelectrically coupled small electric dipoles reside on a triangular lattice. The quantum paraelectric hexaferrite $\text{BaFe}_{12}\text{O}_{19}$, in which small electric dipoles originated from the off-center displacement of Fe^{3+} in the FeO_5 bipyramids constitute a two-dimensional triangular lattice⁴, represents a promising candidate to generate the anticipated electric-dipole liquid. We present a series of experimental evidences, including dielectric permittivity, heat capacity, and thermal conductivity measured down to 66 mK, to reveal the existence of a nontrivial ground state in $\text{BaFe}_{12}\text{O}_{19}$, characterized by itinerant low-energy excitations with a small gap, to which we interpret as an exotic liquid-like quantum phase. The quantum electric-dipole liquids in frustrated dielectrics open up a fresh playground for fundamental physics and may find applications in quantum information and computation as well.

Geometric frustrations arise on various triangle-based lattices like one-dimensional (1D) trestle lattice, two-dimensional (2D) triangular and kagome lattices, three-dimensional (3D) B-site spinel and pyrochlore lattices, and are typically investigated in spin systems¹⁻³. It has become well known that the introduction of quantum fluctuations in geometrically frustrated magnets give rise to a rich variety of interesting quantum phases⁵⁻⁸. Especially, exotic quantum spin liquids (QSLs), characterized by either gapped or gapless itinerant excitations⁸, have been theoretically predicted to show extremely intriguing phenomena. Compared with the impressive progress and diversity in theory, nevertheless, a clear identification of QSLs in real materials has proved challenging, with a very limited number of candidates reported so far⁹⁻¹³.

Similar to the situation of spin lattices in magnets, geometric frustration can occur in lattices made of electric dipoles in dielectrics. In the case of small electric dipoles with significant quantum fluctuations persisted down to $T = 0$ K, exotic disordered quantum phases such as a quantum electric-dipole liquid (QEL), could be anticipated in certain conditions. In fact, some theoretical models proposed for ultracold dipolar particles trapped on 2D frustrated optical lattices have predicted topological quantum phases with fractional excitations¹⁴. In a QEL, the electric dipoles are highly entangled with one another in a form of quantum dimers (pairs of antiparallel dipoles) and continue to fluctuate in the resonating valence bond (RVB) state, a picture qualitatively similar to a QSL. However, we must emphasize that the QEL should have distinctive features from QSLs, because electric dipole and spin have important differences¹⁵. For instance, electric dipole neither has intrinsic angular momentum nor exhibits quantum precession as magnetic dipole (spin) does. Moreover, the nature of short-range and long-range interactions between electric dipoles is very different from that of spins¹⁶. This could lead to a very different phase diagram between QSLs and QELs.

Frustration in dielectrics has been previously studied in materials with competing ferroelectric (FE) and antiferroelectric (AFE) constituents such as the $\text{KH}_2\text{PO}_4/\text{NH}_4\text{H}_2\text{PO}_4$ (KDP-ADP) family or containing random-site impurities like $\text{KTaO}_3:\text{Li}$, which usually result in electric-dipole glasses similar to spin glasses^{17,18}. However, geometric origin of frustrations and cooperative liquid-like quantum phases have been largely ignored in the studies of dielectrics. On another hand, the role of quantum fluctuations in dielectrics has been noticed since 1970s when people were studying the abnormal dielectric behavior of SrTiO_3 (ref. 19). It was proposed that quantum fluctuations in SrTiO_3 prevent the onset of long-range FE order so that a quantum paraelectric state persists down to zero temperature²⁰. Since then, quantum paraelectricity has been reported in a number of perovskite oxides with similar structures to SrTiO_3 , such as CaTiO_3 , EuTiO_3 , KTaO_3 , *etc.* The quantum paraelectrics provide a new playground for the study of quantum critical phenomena¹⁵, but it seems hopeless to search for the QELs in those perovskite quantum paraelectrics because their crystalline structures and FE interactions usually do not introduce geometric frustrations. In this

Letter, we demonstrate that both geometric frustrations and quantum fluctuations can be simultaneously achieved in a unique frustrated dielectric ($\text{BaFe}_{12}\text{O}_{19}$). Our experiments measured down to 66 mK suggest that it has a very unusual liquid-like ground state, characterized by itinerant low-energy excitations with a small gap. We consider this nontrivial quantum phase as a possible candidate of QELs.

Recently we have discovered that the well-known M-type hexaferrites, such as $\text{BaFe}_{12}\text{O}_{19}$, belong to a completely new family of quantum paraelectrics⁴. Other hexaferrites containing the FeO_5 bipyramids in their crystal structures, such as the W-, Z-, X- and U-type hexaferrites, are also likely candidates of quantum paraelectrics⁴. The M-type hexaferrite $\text{BaFe}_{12}\text{O}_{19}$ is one of the most popular magnetic materials with a wide use in magnetic credit cards, bar codes, small motors, and low-loss microwave devices²¹, due to its superior properties of ferrimagnetic ordering with a strong ferromagnetic moment and a very high Néel temperature (~ 720 K), high resistivity, as well as low cost of synthesis. The crystal structure of $\text{BaFe}_{12}\text{O}_{19}$ is shown in Fig. 1a. It can be described by a periodically stacking sequence of two basic building blocks – S block and R block along c axis. The Fe^{3+} ions occupy three different kinds of sites: octahedral, tetrahedral, and bipyramidal sites. In particular, the FeO_5 bipyramids only exist in the middle of the R/R^* blocks and form a triangular lattice in ab plane (Fig. 1b). Previous experiments including Mössbauer spectroscopy²², x-ray diffraction²³, and neutron diffraction²⁴ have revealed the existence of off-equatorial displacements for Fe^{3+} at Wyckoff position of 2b site inside the FeO_5 bipyramids to minimize the total energy, which results in two adjacent Wyckoff positions of 4e sites with a lowered symmetry (Fig. 1c). The off-equatorial displacement (4e-4e distances are 0.176(5) Å at 4.2 K and 0.369(5) Å at room temperature)²² would induce a small local electric dipole P along c axis in each FeO_5 bipyramid (Fig. 1c). A dynamic displacement persists down to the lowest temperature due to the significant quantum tunneling between two 4e sites and the weak dipole-dipole coupling along c axis. Consequently, a quantum paraelectric behavior without long-range electric ordering has been observed in $\text{BaFe}_{12}\text{O}_{19}$ (ref. 4).

More importantly, these electric dipoles associated with the FeO_5 bipyramids reside on a triangular lattice in each R/R^* block. Because the R/R^* blocks are well separated by the S/S^* blocks, this triangular lattice thus has a 2D feature. Consequently, a dielectric system with uniaxial (Ising-type) electric dipoles on a 2D triangular lattice is practically achieved in $\text{BaFe}_{12}\text{O}_{19}$ (Fig. 1c). If the neighboring dipole-dipole interaction favors anti-alignment, the system confronts frustrations and has a very large degeneracy of ground states. In this sense, $\text{BaFe}_{12}\text{O}_{19}$ would be a very unique quantum paraelectric other than those previously known, in which both geometric frustrations and strong quantum fluctuations may play an important role. Thus, the quantum paraelectric $\text{BaFe}_{12}\text{O}_{19}$ sets up a promising candidate to search the anticipated QELs, where an assembly of quantum dimers (pairs of dipoles) with either short-range or long-range entanglement continue to fluctuate (Fig. 1d). We then employ a series of experimental techniques to resolve the ground state of $\text{BaFe}_{12}\text{O}_{19}$.

A prerequisite of a QEL is the AFE interaction between neighboring dipoles. To confirm the AFE coupling in BaFe₁₂O₁₉, we have made a careful analysis on the low-temperature dielectric permittivity. As shown in Fig. 2a, the dielectric permittivity along *c* axis (ϵ_c) of BaFe₁₂O₁₉ increases steadily with decreasing temperature but remains nearly constant below ~ 5.5 K. No dielectric phase transition is observed down to 1.5 K. This dielectric behavior evidences a quantum paraelectricity, similar to that in SrTiO₃. The quantum paraelectric behavior can be well described by the mean-field Barrett formula²⁵:

$$\epsilon = A + \frac{M}{\left(\frac{1}{2}T_1\right) \coth\left(\frac{T_1}{2T}\right) - T_0} \quad (1)$$

where A is a constant, T_0 is proportional to the effective dipole-dipole coupling constant and the positive and negative values correspond to FE and AFE interactions, respectively. T_1 represents the tunneling integral and is a dividing temperature between the low temperature region where quantum fluctuation is important and the high temperature region where quantum effect is negligible. $M = n\mu^2/k_B$, where n is the density of dipoles and μ denotes the local dipolar moment. After fitting the ϵ_c below 160 K to the Barrett formula, we obtained $T_0 = -22.9(1)$ K and $T_1 = 47.3(1)$ K. The negative T_0 confirms the AFE coupling between electric dipoles. We note that recent first-principle calculations²⁸ also predicted the AFE interaction with frustration in BaFe₁₂O₁₉. The relative strength of quantum fluctuations can be estimated by $\sim |T_1/T_0| = 2.06$, which is likely high enough to favor a liquid ground state rather than an ordered or glass phase. The uniaxial anisotropy is evidenced by comparing the dielectric permittivity along *c* axis with that in the *ab*-plane. As seen in the inset of Fig. 2a, the in-plane ϵ decreases slowly with decreasing temperature (less than 1 for a temperature interval of 250 K). The absence of a paraelectric behavior in the *ab*-plane is consistent with the uniaxial electric dipoles along *c* axis.

Further evidences of the AFE coupling in BaFe₁₂O₁₉ are presented in Fig. 2b. For those perovskite quantum paraelectrics with FE coupling, such as SrTiO₃, a moderated electric field is able to drive the quantum paraelectric state into a long-range ordered FE state. In strong contrast, for BaFe₁₂O₁₉, an external electric field of 5 kV/cm applied along *c* axis has no detectable influence on the dielectric permittivity. This inertness to external electric fields may indicate the AFE interaction in BaFe₁₂O₁₉. Moreover, the *P-E* loop at 2 K (the inset of Fig. 2b) shows a nearly linear response with quite small polarization up to a high electric field of 30 kV/cm, further implying the AFE coupling. It should be clarified that the magnetic moments of Fe³⁺ at the bipyramidal sites are all parallel along *c* axis in the *R/R** blocks (see Supplementary Information) so that there are no magnetic frustrations on the triangular lattice^{21,24,26}.

The thermodynamic studies at temperatures as low as possible are crucial to identify the conjectured quantum liquid state, as they provide key informations on the spectrum of low-energy elementary excitations. Heat capacity and thermal transport measurements

can probe the low-energy density of states as well as determine whether these low-energy excitations are localized or itinerant, and have been indispensably employed in the study of QSLs²⁷⁻²⁹.

Since BaFe₁₂O₁₉ is a good insulator (see Supplementary Information) with long-range collinear ferrimagnetic ordering ($T_N=720$ K), both the electronic and magnon contributions to the thermal dynamics become negligible at very low temperatures³⁰. Therefore, its thermodynamics at low enough temperatures should be dominated by the lattice contribution only, and the well-known T^3 dependence would be expected for both the heat capacity and thermal conductivity. Fig. 3a shows the heat capacity (C_P) of BaFe₁₂O₁₉ at low temperatures ($T < 10$ K). No sharp anomaly due to a phase transition could be detected down to 0.4 K, in accordance with the quantum paraelectric behavior. Unfortunately, the heat capacity data become scattered and noisy below ~ 1 K, possibly due to the very small values that reach the resolution limit of our equipment. Thus, a quantitative analysis of the heat capacity data is not possible.

The thermal conductivity provides more reliable and critical information on the low-lying elementary excitations, because it is sensitive exclusively to itinerant excitations and totally insensitive to localized entities that may cause the nuclear Schottky contribution and plague the heat capacity measurements at low temperatures^{28,29}. For example, although the heat capacity study²⁷ suggested a gapless QSL in the frustrated triangular magnet κ -(BEDT-TTF)₂Cu₂(CN)₃, the thermal conductivity measurements²⁸ carried out down to 80 mK clarified instead a gapped QSL in the same material. We then have devoted a great effort to measure precisely the thermal conductivity of BaFe₁₂O₁₉ down to 66 mK.

Fig. 3b shows the thermal conductivity κ measured in *ab*-plane as a function of temperature below ~ 1 K. κ decreases rapidly with cooling, with a change more than 2 orders from 1 K to 100 mK. No anomaly due to a phase transition is observed down to 66 mK. The thermal conductivity divided by temperature as a function of T^2 is plotted in Fig. 3c. The data between 0.65 and 1 K exactly follow a linear relation with an extrapolation to the origin, in a good agreement with what expected for the phonon thermal conductivity, $\kappa = \beta T^3$, with $\beta = 0.098 \text{ WK}^{-4}\text{m}^{-1}$. Nevertheless, there is apparently an extra contribution below ~ 650 mK in addition to the normal phonon term, strongly suggesting the existence of abundant itinerant low-energy excitations other than phonons. Moreover, the thermal transport behavior at the zero temperature limit provides key information on the nature of these low-lying excitations. As seen in Fig. 3d, κ/T in the $T \rightarrow 0$ K limit tends to vanish rather than having a finite residual value, immediately implying the absence of gapless excitations. Instead, the data at the lowest temperature regime ($T < 125$ mK) can be fitted to

$$\kappa = \alpha \exp(-\Delta/k_B T) + \beta T^3 . \quad (2)$$

The inset of Fig. 3 shows an Arrhenius plot of $\kappa^* = \kappa - \beta T^3$ in the lowest temperature region. The good linearity confirms the validity of Eq. (2). The best fit gives $\Delta = 0.16(1)$ K, which is much smaller than the effective dipole-dipole interaction constant T_0 (~ 22 K).

The exponential behavior of thermal conductivity at the zero temperature limit is very similar to that observed in the frustrated triangular magnet κ -(BEDT-TTF)₂Cu₂(CN)₃ where a QSL with gapped excitations ($\Delta = 0.46$ K) was identified²⁹. Therefore, the thermal transport behavior excludes a frozen dipole glass or a classical paraelectric phase but strongly suggests an exotic liquid-like ground state.

In order to exclude the possibility that these itinerant low-lying excitations may have a magnetic origin, we further studied the influence of magnetic field on the thermal conductivity behavior. As seen in Fig. 3d, a high magnetic field of 14 T applied along the easy c axis has no influence on the in-plane thermal conductivity in the lowest temperature range. The inertness of these low-lying excitations to external magnetic fields supports our argument that they stem from electric dipoles rather than spins.

Based on above experimental results, especially the thermal conductivity at the zero temperature limit, we conclude that an exotic ground state is likely established in the geometrically frustrated quantum paraelectric BaFe₁₂O₁₉. This liquid-like quantum phase is characterized by itinerant low-energy excitations with a small gap, which could be a candidate of anticipated QELs. As present transverse Ising models proposed for frustrated spin systems on a triangular lattice are inadequate for the frustrated electric dipoles with long-range interactions, a quantitative comparison between experiments and theories is not available at this stage. We expect that our experimental findings will stimulate theoretical efforts towards this subject. The present work serves as a start point of a fresh field and an abundance of exotic phenomena associated with geometrically frustrated quantum electric dipoles are awaiting ahead.

Methods:

Sample preparation. The single crystal samples of BaFe₁₂O₁₉ were prepared by flux method and characterized with x-ray diffraction, as shown in Supplementary Fig. S1. Powders of BaCO₃, Fe₂O₃ and fluxing agent Na₂CO₃ were weighed to molar ratio of 1:1:1, then were mixed and well ground. The ground raw powder was put in Pt crucible and heated to 1250 °C for 24 h in the air, then cooled down to 1100 °C at a rate of 3 °C/min and finally quenched to room temperature.

Dielectric measurements. The dielectric measurements were carried out in a Cryogen-free Superconducting Magnet System (Oxford Instruments, TeslatronPT) down to 1.5 K. To measure the dielectric permittivity, silver paste was painted on the surfaces of a thin plate of crystal and annealed at 150 °C for about 30 mins to make good electrodes. An Agilent 4980A LCR meter was used to measure the dielectric permittivity with the frequency $f = 1$ MHz.

Heat capacity and thermal transport measurements. Heat capacity measurements were performed down to 0.4 K in a commercial Physical Properties Measurement System (PPMS, Quantum Design) using a ³He refrigerator. A thin-plate shaped sample with mass of 12.7 mg was used for this measurement. The contribution of attendant was measured

separately and subtracted from the raw data. Thermal conductivity was measured between 60 mK and 1 K using the conventional steady-state “one heater, two thermometers” technique in a ^3He - ^4He dilution refrigerator (for details, see Zhao et al. *Phys. Rev. B* **91**, 134420 (2015)). A parallelepiped-shaped sample with size of $2.0 \times 0.57 \times 0.11 \text{ mm}^3$ was cut from the as-grown crystals for thermal conductivity measurements.

References

1. Ramirez, A. P. Strongly geometrically frustrated magnets. *Annual Review of Materials Science* **24**, 453-480 (1994).
2. Moessner R. & Ramirez, A. P. Geometrical frustration. *Physics Today* **59**, 24-29 (2006).
3. Balents, L. Spin liquids in frustrated magnets. *Nature* **464**, 199-208 (2010).
4. Shen, S. *et al.* Magnetic-ion-induced displacive electric polarization in FeO_5 bipyramidal units of $(\text{Ba,Sr})\text{Fe}_{12}\text{O}_{19}$ hexaferrites, *Phys. Rev. B* **90**, 180404(R) (2014).
5. Moessner, R., Sondhi, S. L. & Chandra, P. Two-dimensional periodic frustrated Ising models in a transverse field. *Phys. Rev. Lett.* **84**, 4457-4460 (2000).
6. Moessner, R. & Sondhi, S. L. Ising models of quantum frustration. *Phys. Rev. B* **63**, 224401 (2001).
7. Moessner, R. & Sondhi, S. L. Resonating valence bond phase in the triangular lattice quantum dimer model. *Phys. Rev. Lett.* **86**, 1881-1884 (2001).
8. Wen, X-G. Quantum orders and symmetric spin liquids. *Phys. Rev. B* **65**, 165113 (2002).
9. Shimizu, Y., *et al.* Spin liquid state in an organic Mott insulator with a triangular lattice. *Phys. Rev. Lett.* **91**, 107001 (2003).
10. Lee, S. H., *et al.* Quantum-spin-liquid states in the two-dimensional kagome antiferromagnets $\text{Zn}_x\text{Cu}_{4-x}(\text{OD})_6\text{Cl}_2$. *Nat. Mater.* **6**, 853-857 (2007).
11. Okamoto, Y., *et al.* Spin-liquid state in the $S=1/2$ hyperkagome antiferromagnet $\text{Na}_4\text{Ir}_3\text{O}_8$. *Phys. Rev. Lett.* **99**, 137207 (2007).
12. Han, T. H., *et al.* Fractionalized excitations in the spin-liquid state of a kagome-lattice antiferromagnet. *Nature* **492**, 406-410 (2012).
13. Clark, L., *et al.* Gapless spin liquid ground state in the $S=1/2$ vanadium oxyfluoride kagome antiferromagnet $[\text{NH}_4]_2[\text{C}_7\text{H}_{14}\text{N}][\text{V}_7\text{O}_6\text{F}_{18}]$. *Phys. Rev. Lett.* **110**, 207208 (2013).
14. Sun, K., Zhao, E. & Liu, W. V. Topological phases of dipolar particles in elongated Wannier orbitals. *Phys. Rev. Lett.* **104**, 165303 (2010).
15. Rowley, S. E. *et al.* Ferroelectric quantum criticality. *Nat. Phys.* **10**, 367-372 (2014).
16. Baranov, M., Dalmonte, A., Pupillo, M. G. & Zoller, P. Condensed matter theory of dipolar quantum gases. *Chem. Rev.* **112**, 5012-5061 (2012).
17. Courtens, E. Vogel-Fulcher scaling of the susceptibility in a mixed-crystal proton glass. *Phys. Rev. Lett.* **52**, 69-72 (1984).

18. Vugmeister, B. E. & Glinchuk, M. D. Dipole glass and ferroelectricity in random-site electric dipole systems. *Rev. Mod. Phys.* **62**, 993-1026 (1990).
19. Müller, K. A. & Burkhard, H. SrTiO₃: An intrinsic quantum paraelectric below 4 K. *Phys. Rev. B* **19**, 3593-3602 (1979).
20. Prosandeev, S. A., Kleemann, W., Westwanski, B. & Dec, J. Quantum paraelectricity in the mean-field approximation. *Phys. Rev. B* **60**, 14489-14491 (1999).
21. Pullar, R. C. Hexagonal ferrites: A review of the synthesis, properties and applications of hexaferrite ceramics, *Prog. Mat. Sci.* **57**, 1191-1334 (2012).
22. Albanses, G., Deriu, A. & Cabrini, D. The dynamics of iron ions in pseudotetrahedral (bipyramidal) sites of BaFe₁₂O₁₉ and SrFe₁₂O₁₉ hexagonal ferrites. *Hyperfine Interactions* **70**, 1087-1090 (1992).
23. Obradors, X., Collomb, A., Pernet, M., Samaras, D. & Joubert, J. C. X-ray analysis of the structural and dynamic properties of BaFe₁₂O₁₉ hexagonal ferrite at room temperature. *J. Solid State Chem.* **56**, 171-181 (1985).
24. Cao, H. B., *et al.* High pressure floating zone growth and structural properties of ferrimagnetic quantum paraelectric BaFe₁₂O₁₉. *APL Materials* **3**, 062512 (2015).
25. Barrett, J. H. Dielectric constant in perovskite type crystals. *Phys. Rev.* **86**, 118120 (1952).
26. Wang, P. S. & Xiang, H. J. Room-temperature ferrimagnet with frustrated antiferroelectricity: promising candidate toward multiple-state memory. *Phys. Rev. X* **4**, 011035 (2014).
27. Yamashita, S., *et al.* Thermodynamic properties of a spin-1/2 spin-liquid state in a κ-type organic salt. *Nat. Phys.* **4**, 459-462 (2008).
28. Yamashita, M., *et al.* Thermal-transport measurements in a quantum spin-liquid state of the frustrated triangular magnet κ-(BEDT-TTF)₂Cu₂(CN)₃. *Nat. Phys.* **5**, 44-47 (2009).
29. Yamashita, M. *et al.* Highly mobile gapless excitations in a two-dimensional candidate quantum spin liquid. *Science* **328**, 1246-1248 (2010).
30. Hess, C. *et al.* Magnon heat transport in doped La₂CuO₄. *Phys. Rev. Lett.* **90**, 197002 (2003).

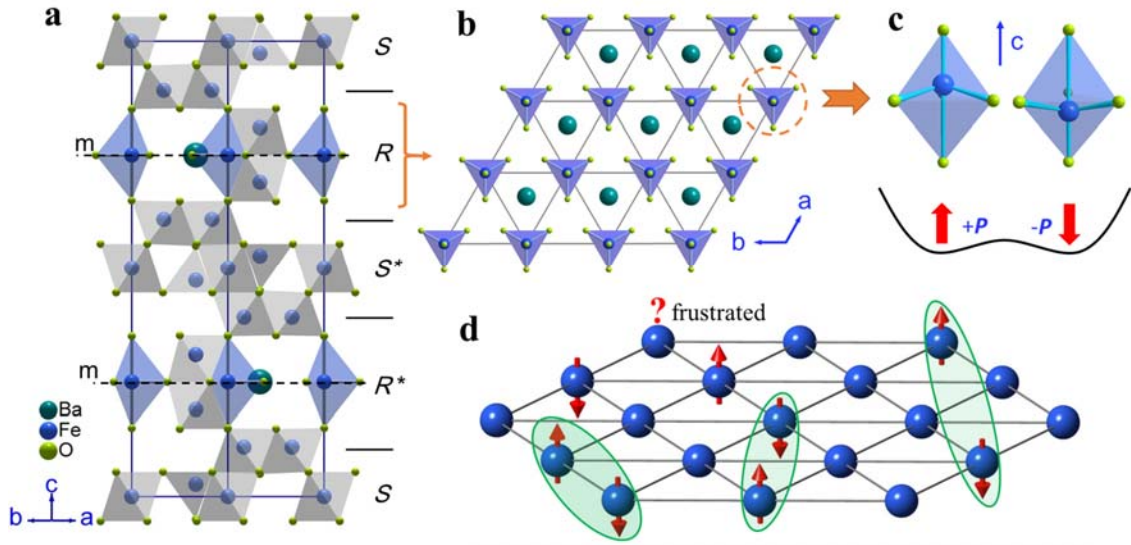


Figure 1 Uniaxial electric dipoles on a triangular lattice in BaFe₁₂O₁₉. (a) Crystal structure of the M-type hexaferrite BaFe₁₂O₁₉. It consists of alternate stacks of *S* and *R* blocks along *c* axis. The asterisk symbols indicate that the corresponding blocks rotate about *c* axis by 180°. The Fe³⁺ ions occupy three different sites: octahedral, tetrahedral, and bipyramidal (blue) sites. A mirror plane (*m*) bisects equally the bipyramids in the *R/R** blocks. (b) The 2D triangular lattice of FeO₅ bipyramids in each *R/R** block. (c) Illustration of Fe³⁺ off-equator displacements in the FeO₅ bipyramid. The upward or downward displacements at two 4e sites give rise to small electric dipoles along *c* axis. Quantum fluctuations between two 4e sites persist to *T*=0 K. (d) Frustrated electric dipoles on a triangular lattice. Each site contains an Ising-type electric dipole while the neighboring interactions favor anti-alignment. Quantum dimers with either short-range or long-range entanglement continue to fluctuate and results in a QEL.

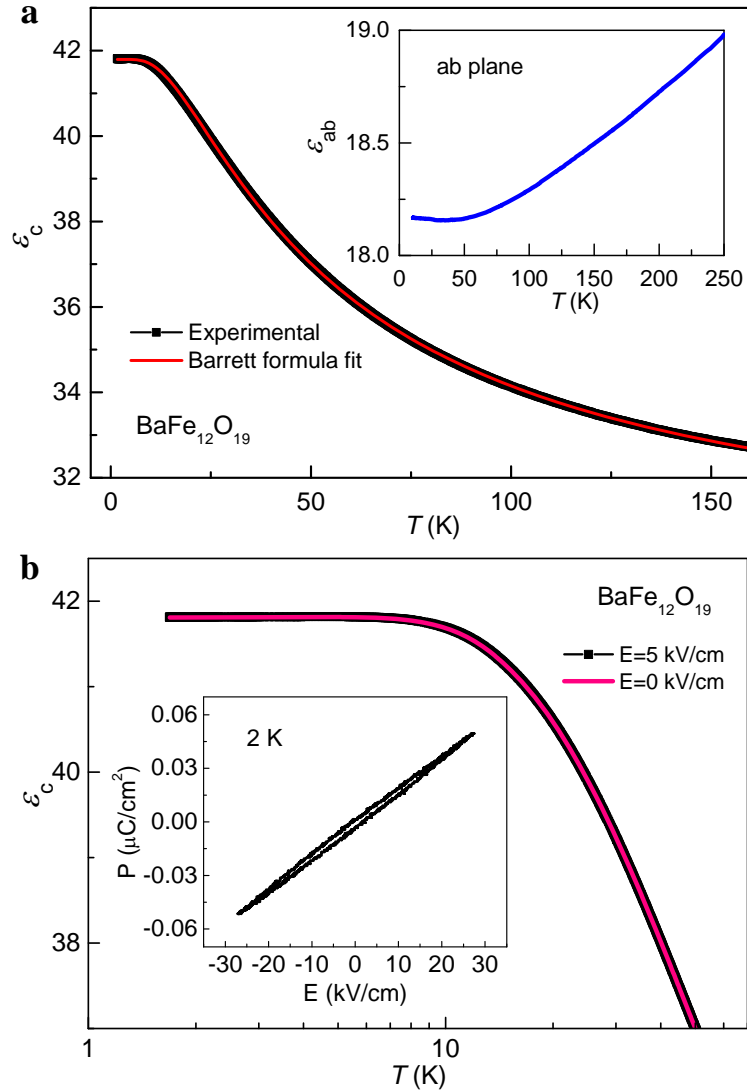


Figure 2 Dielectric permittivity of BaFe₁₂O₁₉. (a) The temperature dependence of *c*-axis dielectric permittivity ϵ_c . The red solid line is the fitting curve to the Barrett formula. The negative fitting parameter $T_0 = -22.9(1)$ K suggests the AFE interaction. The inset shows the dielectric permittivity measured along the [100] direction in *ab*-plane. (b) The temperature dependence of dielectric permittivity ϵ_c measured with DC bias electric fields. A bias electric field of 5 kV/cm has no detectable influence on the quantum paraelectric behavior. The inset shows the P - E loop at 2 K. The nearly linear response and the low values of P imply the AFE coupling.

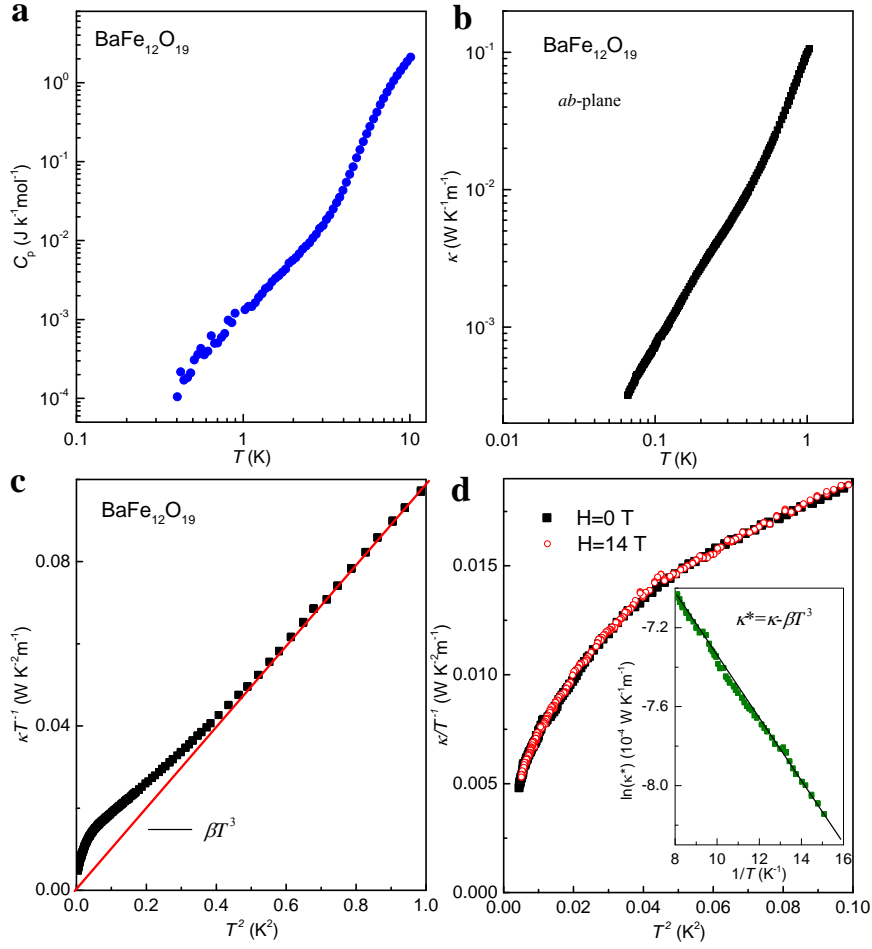


Figure 3 Heat capacity and thermal conductivity of BaFe₁₂O₁₉. (a) Heat capacity C_p as a function of temperature. No phase transition is detected down to 0.4 K. (b) Thermal conductivity κ measured in ab -plane as a function of temperature. No anomaly due to a phase transition is observed down to 66 mK. (c) The ab -plane thermal conductivity divided by temperature plotted as a function of T^2 below ~ 1 K. The red solid line represents the expected thermal conductivity of phonons, $\kappa = \beta T^3$, with $\beta = 0.098$ WK⁻⁴m⁻¹. Apparently, there is an extra contribution beside the phonon thermal conductivity below ~ 650 mK. (d) The κT^{-1} versus T^2 plot in the lowest temperature region. κ/T tends to vanish at the $T \rightarrow 0$ K limit. An applied magnetic field of 14 T along c axis has no influence on the ab -plane thermal conductivity in this low-temperature region. The inset shows the Arrhenius plot of $\kappa^* = \kappa - \beta T^3$ below ~ 125 mK. The good linearity suggests gapped excitations with a small gap ~ 0.16 K.

Supplementary Information

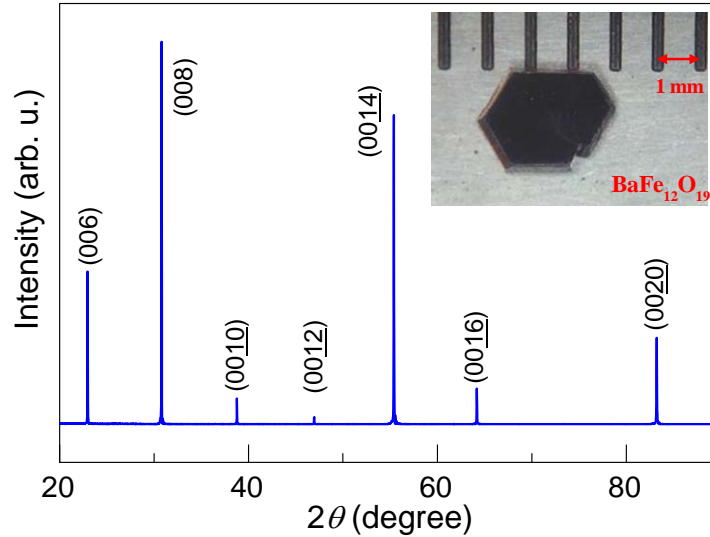


Fig. S1 The single-crystal x-ray diffraction pattern of BaFe₁₂O₁₉ at room temperature. The inset shows a picture of flux-grown single crystals.

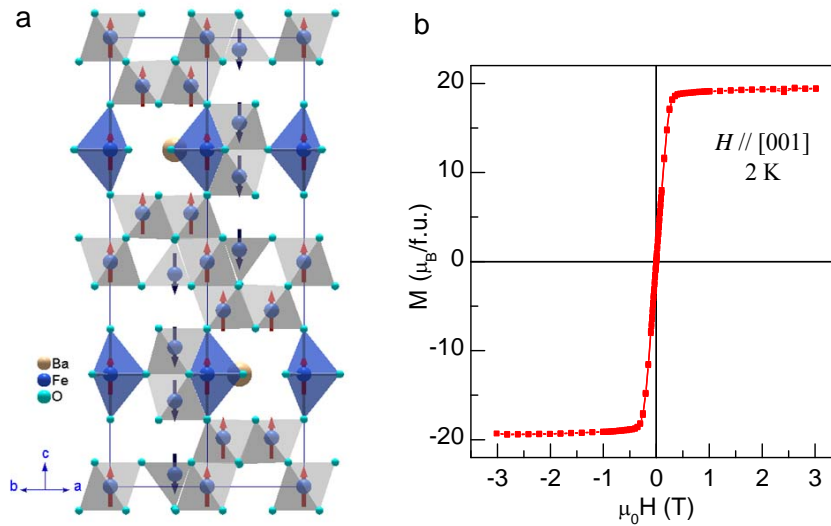


Fig. S2 (a) Magnetic structure of BaFe₁₂O₁₉. The magnetic moments at the FeO₅ bipyramidal sites are parallel to each other so that there is no magnetic frustration on the triangular lattice. (b) The M - H hysteresis curve of BaFe₁₂O₁₉ measured at 2 K along c axis. It is consistent with a long-range collinear ferrimagnetic ordering.

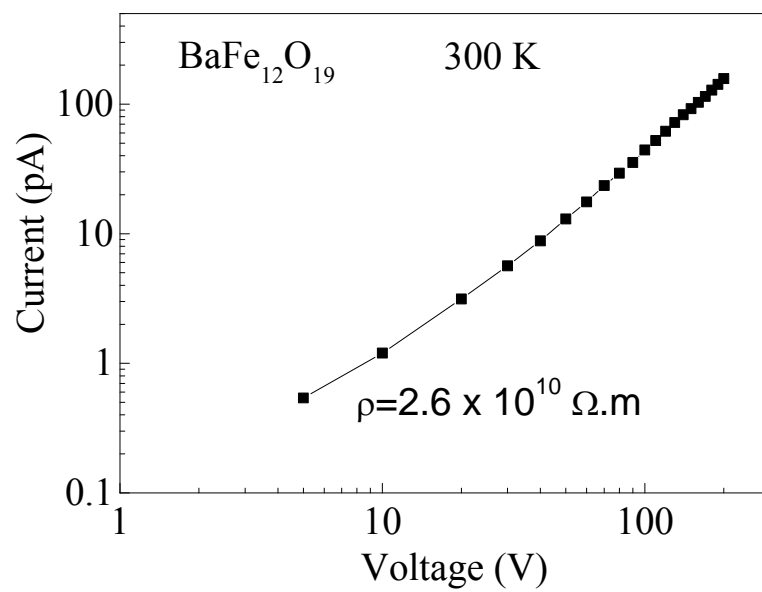


Fig. S3 I-V characteristic and resistivity along c axis of BaFe₁₂O₁₉ measured at room temperature. The sample is highly insulating even at room temperature, suggesting a good quality of the grown single crystals.